Journal of Molecular Structure 1296 (2024) 136910

Contents lists available at ScienceDirect

Journal of Molecular Structure

journal homepage: www.elsevier.com/locate/molstr

Molecular structure and internal dynamics of the antioxidant 2,6-di-tert-butylphenol

Wenqin Li [a], Assimo Maris [b], Sonia Melandri [b], Alberto Lesarri [a,*], Luca Evangelisti [c,*]

[a] Departamento de Química Física y Química Inorgánica, Facultad de Ciencias—I.U. CINQUIMA, Universidad de Valladolid, Paseo de Belén 7, Valladolid 47011, Spain
[b] Department of Chemistry "G. Ciamician", University of Bologna, Via F. Selmi 2, Bologna 40126, Italy
[c] Department of Chemistry "G. Ciamician", University of Bologna, Via S. Alberto 163, Ravenna 48123, Italy

ARTICLE INFO

Keywords:
Antioxidant
Molecular structure
Rotational spectroscopy
Supersonic jet spectroscopy

ABSTRACT

Antioxidants are a class of chemical compounds with particular chemico-physical properties that make them suitable for reducing oxidative stress. In this work we report the rotational spectroscopy analysis of the antioxidant 2,6-di-tert-butylphenol in a jet expansion. The rotational spectrum reveals both fine and hyperfine tunnelling components. The largest spectral doubling consists of two distinct groups of lines separated by ~190 MHz, and is due to the torsional motion associated with the hydroxyl group. Each component of the doublet is further split into three fine components, with separations below 1 MHz. The spectrum was reproduced with a two-state torsion-rotation semirigid Hamiltonian for each pair of torsional states. Additional observation of all the singly-substituted ^{13}C isotopologues allowed to determine the substitution structure by means of the Kraitchman equations. The comparison with the equilibrium structure obtained by computational calculations at B3LYP-D3BJ/def2-TZVP level validate the accurate determination of the carbon skeleton and tert-butyl group positions. The investigation of intramolecular dynamics with a monodimensional flexible model demonstrates that the tunnelling phenomenon arises from the hydroxyl group's equivalent positions, with a double-minimum potential separated by a barrier of 1000(100) cm^{-1} allowing for this large amplitude motion. However, the threefold fine structurte, while plausibly associated to internal motions within the tert-butyl group, will require further exploration.

1. Introduction

Materials are constantly exposed to oxidative stress resulting from sunlight exposure, atmospheric oxygen, or adverse environmental conditions. This oxidative stress induces the formation of reactive oxygen species (ROS), including oxygen radicals such as hydroxyl ($HO^{\cdot}$), superoxide anion ($O_2^{\cdot-}$), alkoxyl radicals ($RO^{\cdot}$), and peroxyl radicals ($ROO^{\cdot}$). Additionally, nonradical oxidants, such as hydrogen peroxide (H_2O_2), singlet oxygen ($^1O_2$), hypochlorous acid (HOCl), and peroxynitrite ($ONOO^-$), can easily convert into radicals [1]. The presence of ROS can lead to various modifications in materials, causing diseases in living tissues or altering the chemical and physical properties of nonliving materials. To counteract oxidative processes and protect materials, antioxidants play a vital role [2]. Antioxidants are molecular compounds that possess the ability to neutralize free radicals, thereby inhibiting oxidative reactions and safeguarding the integrity of materials. These compounds are abundantly present in nature, and even small concentrations can effectively preserve the properties of a system. Phenolic compounds (PCs) are a significant group of naturally occurring antioxidants found in fruits, vegetables, and other sources. They serve as vital nutrients for animals and are employed by humans as food preservatives or for various industrial purposes [3]. PCs, including flavonoids, stilbenes, lignans, and phenolic acids, exhibit antioxidant activity, which is closely linked to their structural properties, particularly the number and arrangement of hydrogen groups and other substitutions. In this study, we focus on investigating the structural properties of a specific antioxidant called 2,6-di-tert-butylphenol (26BP) using rotational spectroscopy. Rotational spectroscopy has long been utilized to analyse gaseous molecules, enabling the determination of molecular structures and identification of different isomers, even in complex mixtures, helping comparison with computational calculations [4]. Notably, rotational spectroscopy has been successfully employed to characterize essential antioxidants like various conformers of vitamin C stabilized by distinct intramolecular hydrogen bonding [5], five

* Corresponding authors.
E-mail addresses: alberto.lesarri@uva.es (A. Lesarri), luca.evangelisti6@unibo.it (L. Evangelisti).

https://doi.org/10.1016/j.molstruc.2023.136910
Received 30 May 2023; Received in revised form 16 October 2023; Accepted 19 October 2023
Available online 20 October 2023

conformers of 1,3-propanedithiol which is the pharmacofore of the dihydrolipoic acid [6], a powerful cellular antioxidant, and 3 conformers of N,N-diethylhydroxylamine [7–9], an oxygen scavenger largely used in water treatment. The technique has advanced over the years, allowing the analysis of increasingly larger molecules. Consequently, we have chosen to apply rotational spectroscopy to study 26BP, an antioxidant widely used in the petrochemical and plastic industries. 26BP belongs to the category of "radical scavengers" as it directly reacts with free radicals in a system, effectively retarding the degradation process by generating more stable radicals. Two main mechanisms have been proposed to describe its antioxidant action [10]. In the first mechanism, the antioxidant transfers the hydroxyl hydrogen to the radical, becoming a radical itself:

$$R^{\cdot} + PhOH \rightarrow RH + PhO^{\cdot}$$

The bond dissociation energy (BDE) is commonly used as a descriptor to evaluate this antioxidant action, as the ease of breaking the O—H bond correlates with the inactivation of the radical.

The second proposed mechanism involves electron abstraction:

$$R^{\cdot} + PhOH \rightarrow R^{-} + PhO^{\cdot +}$$

In this case, the ionization potential (IP) serves as the descriptor, with lower IP values indicating easier electron abstraction.

In this study we present the rotational spectrum of 26BP, which can be directly compared to the phenol prototype [11–14] due to their similar structural frameworks. As in other symmetrically substituted derivatives [15], the intramolecular dynamics associated to the double-minimum torsional motion of the alcohol group is expected to produce tunnelling splitings in the spectrum. This spectral information, quite sensitive to the potential barrier height, can provide information on the torsional potential function for the global minimum [16,17]. By applying rotational spectroscopy, we aim to gain insights into the dynamical behaviour of the hydroxyl group as its chemical environment varies [18], focusing on the structural and electronic characteristics of 26BP.

2. Experimental and computational methods

The experimental analysis was conducted on a sample of 2,6-di-tert-butylphenol (CAS:128–39–2, InChIKey: DKCPKDPYUFEZCP-UHFFFAOYSA-N), obtained as an odourless, colourless solid from Sigma-Aldrich. The declared purity of the sample is larger than 97 %. Due to the high resolution of the rotational spectroscopy technique, no further purification of the sample was necessary.

The rotational spectrum was recorded using a broadband (chirp) Fourier transform spectrometer at the University of Valladolid. The spectrometer is based on the implementation proposed by Pate et al. [19]. The sample, which has a melting point around 309 K and a boiling point of 526 K, was placed in a Parker (Series 9) solenoid injector model and heated to 403 K. The vapours generated *in situ* were diluted with a mixture of argon and helium (1:1) at 0.3 MPa. The resulting gaseous mixture was pulsed into a high vacuum chamber (final pressure ~0.01–0.1 mPa) to produce a supersonic jet. The gas pulse had a duration of approximately 0.5 ms and a repetition rate of 5 Hz. The primary purpose of this expansion is to cool the molecular sample to a rotational temperature of about 1 K, simplifying the spectrum and enhancing its intensity.

After the expansion, the spectrometer employed a fast arbitrary waveform generator to produce a chirp for linear fast passage lasting approximately 4 μs, with a sampling rate of 25 Gsamples/s. The chirps were amplified by a 200 W amplifier for the 2 - 8 GHz measurement range. The microwave radiation induced a polarization through the fast-passage mechanism, followed by rotational decoherence upon emission of a free-induction decay (FID). The FID was amplified by a low-noise amplifier and recorded in the time domain using a digital oscilloscope at a sampling rate of 25 Gsamples/s. The entire electronic sequence was repeated eight times for each molecular pulse. Ultimately, a spectrum consisting of 1.5 M averages was obtained and analysed. The frequency-domain spectrum was obtained by Fourier transforming the 40 μs FID using a Kaiser-Bessel apodization window. Typically, the uncertainty of the frequency measurements and resulting linewidths at full width at half-maximum were 20 kHz and 100 kHz, respectively.

In order to guide the experimental assignment, various computational calculations were performed using density functional theory (DFT) [20] implemented in Gaussian16 [21]. These calculations included the B3LYP method with the addition of the D3 corrections developed by Grimme *et al.*, along with the Becke-Johnson damping function [22,23]. For this calculation, the Weigend and Ahlrich's def2-TZVP basis set was employed [24], as previous researches has demonstrated its accuracy for rotational spectroscopic purposes [25,26]. Subsequently, the results were re-optimized using Møller-Plesset terms up to second order (MP2) with the 6–311++*G*(d,p) basis set [27]. Table 1 presents the spectroscopic parameters obtained from these different methods, including the rotational constants and dipole moment components, which are prerequisite for predicting the rotational spectrum. The frequency calculation at B3LYP-D3BJ/def2-TZVP level was performed within the harmonic approximation. All theoretical predicted structures are reported in the supplementary material.

Table 1
Theoretical and experimental rotational constants of 26BP. The figure at the bottom shows the calculated structure of 26BP and the labelling of each C atom. The blue arrow shows the total electric dipole moment of the conformer.

	MP2/6–311++*G*(d,p)	B3LYPD3BJ/def2TZVP	Experimental
A / MHz	1093.15	1099.52	1092.39844 (14)[a]
B / MHz	403.66	403.89	402.926229(80)
C / MHz	339.86	340.48	339.381923(83)
D_j / Hz		3.3	3.22(44)
ΔE_{01} / MHz			190.20487(79)
$F_{ab,01}$ / MHz			0.8609(32)
ΔE_{23} / MHz			190.02504(78)
$F_{ab,23}$ / MHz			0.8902(31)
ΔE_{45} / MHz			190.74947(78)
$F_{ab,45}$ / MHz			0.8620(22)
σ[b] / kHz			9
N[c]			841
$\mu_a/\mu_b/\mu_c$ [d] / D	1.9/−0.2/0.0	1.8/−0.3/0.0	y/y/n

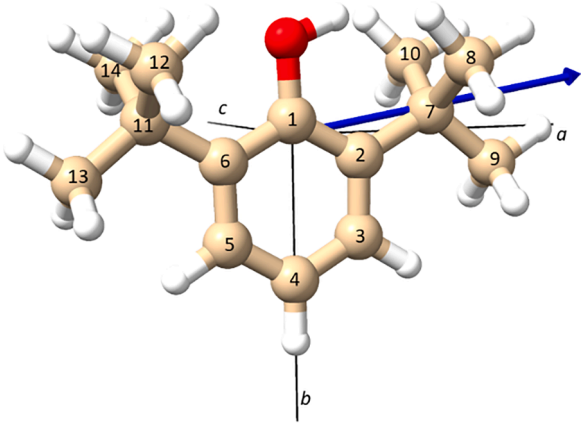

[a] Errors in parentheses are expressed in units of the last digits.
[b] Standard deviation of the fit.
[c] number of fitted transitions.
[d] $\mu_a/\mu_b/\mu_c$ are the electric dipole moments components along the principal inertial axes *a, b* and *c*.

3. Results and discussion

3.1. Rotational spectrum

The molecule has a phenol-like structural skeleton, consisting of a hydroxyl group directly connected to a benzene ring. Two tert-butyl groups are symmetrically attached to the benzene ring at positions 2 and 6, preserving the two-fold symmetry of the torsional potential function.

The rotational spectrum is shown in Fig. 1, revealing a single isomer. The spectrum was analysed considering the dipole moment component μ_a as being predicted to be the most intense. Accordingly, a series of transitions split into fine and hyperfine components was identified. The primary splitting, approximately 190 MHz, separates the transitions into two distinct groups. This splitting arises from the tunnelling motion associated with the hydroxyl group, similar to what is observed in molecules with a similar structural framework, such as phenol [14]. In our case, however, each individual transition was further split into three hyperfine components, which will be described in more detail later. These splittings correspond to three pairs of torsional states labelled as 0–1, 2–3, and 4–5, as shown in Fig. 2.

As in phenol, the μ_a transitions are torsionally interstate, because of the dipole moment inversion associated to the motion along this axis. In addition to the μ_a-type transitions in the R-branch lines, weak transitions of μ_b-type were also observed, which did not exhibit the same small splitting. The μ_b transitions are torsionally intrastate. No transitions of μ_c-type were observed.

All transitions were fitted using Watson's S-reduced Hamiltonian [28] in the I^r representation, employing a semi-rigid rotor term (H^R) common to all states. For each pair of torsional states an additional two-state torsion-rotation coupled Hamiltonian was employed, which yielded a specific torsional energy difference ΔE and a Coriolis coupling term F_{ab}, determined in the reduced-axis system proposed by Pickett [29]:

$$H = H^R + \sum H_{ij}^{int} \quad (1)$$

where:

$$\begin{aligned} H_{ij}^{int} &= \Delta E_{ij} + F_{ab,ij}(P_a P_b + P_b P_a) \\ \text{with } ij &= 01,\ 23 \text{ or } 45 \end{aligned} \quad (2)$$

and where P_α (with α can be *a, b* or *c*) represents the angular momentum operators. The final results are reported in Table 1.

Subsequently, a relatively small set of rotational transitions for each ^{13}C isotopologue was observed and measured in natural abundance (ca. 1 %). The resulting spectroscopic parameters are provided in Table 2, while a complete list of rotational transitions for all the species, along with the corresponding quantum numbers and residual errors, can be found in the supplementary material.

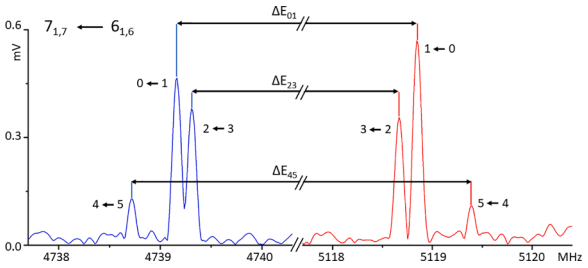

Fig. 2. Characteristic fine structure components of a rotational transition of the normal species of 26BP. Note the main splitting of around 190 MHz and the triplet structure of each minor component.

3.2. Molecular structure

Rotational spectroscopy is a high-resolution technique that can detect distinct rotational spectra for small mass variations, even for isotopologues, as depicted in Fig. 1. The differences in moments of inertia amongst the isotopologues allow for the determination of rotational constants, which, in turn, provide valuable structural information for the molecule.

In the observed spectrum, 12 isotopologues were successfully assigned, and their spectroscopic parameters are presented in Table 3. Several interesting observations can be made:

(a) The motion of the hydroxyl group is revealed by the equivalence of the two hydrogen positions. This symmetry is maintained when replacing position 1 or position 4 with ^{13}C. Consequently, the rotational spectrum retains the fundamental splitting due to the hydroxyl group tunnelling, along with the minor splittings evident in Fig. 2. Due to the relatively low intensity of the experimental spectra for these observed isotopologues, the fitting was performed only for the most intense component.

(b) The 26BP rotational spectrum after ^{13}C-substitution at position 1 is significantly affected by the torsional motion of the hydroxyl group. This vibrational effect is highlighted by the increase in rotational constant *B* when transitioning from ^{12}C to ^{13}C, despite the mass increase. Similar vibrational effects are observed when a deuterium atom replaces a hydrogen atom involved in a hydrogen bond. Additionally, the tunnelling parameter ΔE is

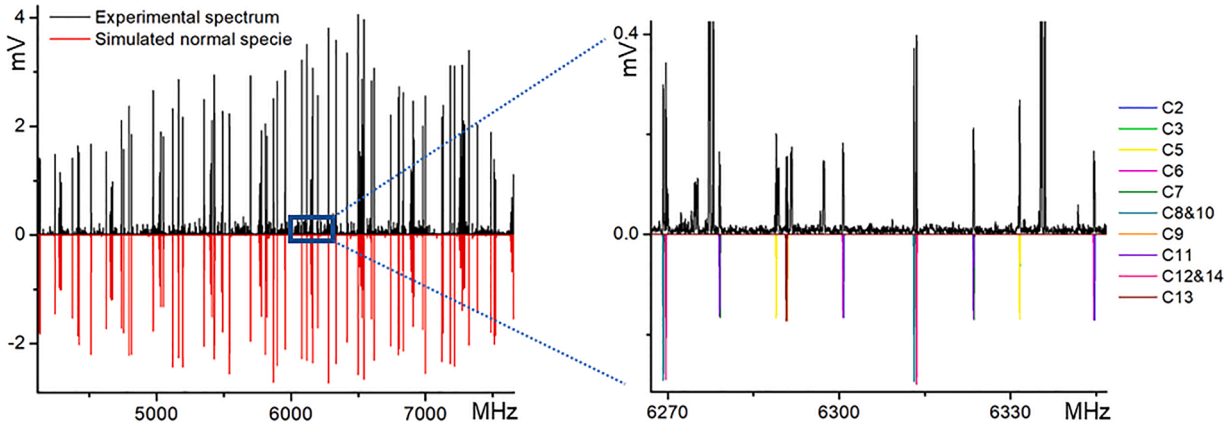

Fig. 1. Broadband rotational spectrum of 26BP. On the left, the black upper trace corresponds to the experimental spectrum (average of 1.5 M FIDs). The lower red trace represents the simulated normal species produced with the experimental spectroscopic parameters at a rotational temperature of 1 K, and the theoretical dipole moment components reported in Table 1. On the right, parts of the spectrum illustrate representative transitions from each of the ^{13}C isotopologues of 26BP in natural abundance.

Table 2
Experimental rotational constants (*S*-reduced Hamiltonian and I^r-representation) of the observed ^{13}C isotopologues of 26BP in natural abundance.

	C1	C2	C3	C4	C5	C6
A / MHz	1092.28(2)	1091.99(1)	1084.60(3)	1077.59(2)	1084.59(3)	1091.97(2)
B / MHz	402.9414(3)	402.4512(3)	402.4588(5)	402.9213(4)	402.4603(5)	402.4423(4)
C / MHz	339.3800(3)	339.0073(2)	338.2987(5)	337.9363(3)	338.2985(5)	338.9999(3)
ΔE_{01} / MHz	189.471(2)			190.204(2)		
$F_{ab,01}$ / MHz	0.99(4)			0.95(5)		
$\sigma^{[b]}$ / kHz	8	10	17	14	18	13
$N^{[c]}$	21	51	48	43	48	54
	C7	C8/C10	C9	C11	C12/C14	C13
A / MHz	1092.17(3)	1085.329(8)	1091.45(2)	1092.16(3)	1085.321(8)	1091.45(1)
B / MHz	400.8136(5)	400.0342(1)	398.4062(3)	400.8059(5)	400.0819(1)	398.3891(2)
C / MHz	337.8582(5)	337.3702(1)	336.0816(3)	337.8540(5)	337.3938(1)	336.0709(2)
$\sigma^{[b]}$ / kHz	18	4	10	19	4	7
$N^{[c]}$	54	57	50	56	57	53

Table 3
Experimental substitution coordinates (r_s) and theoretical equilibrium coordinates (r_e, at B3LYP-D3BJ/def2-TZVP level of theory).

	a (Å)		*b* (Å)		*c* (Å)	
	$\|r_s\|$	r_e	$\|r_s\|$	r_e	$\|r_s\|$	r_e
C1	0	−0.006	0.228(11)	−0.250	0	0.0
C2	1.216(2)	1.231	0.409(6)	0.422	0	0.0
C3	1.202(3)	1.195	1.824(2)	1.816	0	0.0
C4	0.123(25)	0.000	2.522(1)	2.512	0	0.0
C5	1.200(3)	−1.199	1.825(2)	1.818	0	0.0
C6	1.227(2)	−1.242	0.417(7)	0.427	0	0.0
C7	2.573(1)	2.577	0.317(12)	−0.327	0	0.0
C8/C10	2.730(1)	2.729	1.190(1)	−1.188	1.274(1)	±1.274
C9	3.773(1)	3.769	0.636(4)	0.642	0	0.0
C11	2.577(1)	−2.582	0.317(1)	−0.326	0	0.0
C12/C14	2.706(1)	−2.707	1.201(1)	−1.198	1.266(1)	±1.265
C13	3.780(1)	−3.776	0.634(2)	0.640	0	0.0

reduced by ~0.5 MHz respect the normal species, while it remains nearly unchanged in the $^{13}C4$ isotopologue.

(c) By monoisotopically replacing the other carbons, the positions of the hydroxyl group are no longer equivalent, resulting in distinct spectra for each isotopologue, consistent with the symmetry C_s. Notably, the relative intensity of the isotopologue spectra is higher than expected since there is no splitting in the observed transitions.

(d) Positions 8 with 10 and 12 with 14 are equivalent due to the preserved molecular symmetry. Consequently, the rotational spectra of these isotopologues exhibit twice the intensity compared to the spectra of other monosubstituted carbons.

Various methods have been developed over the years to determine the positions of the atoms within the molecule. One widely used approach is the application of Kraitchman's equations [30], which yield the structure r_s. The key advantage of this method is that it does not rely on *a priori* assumptions [31], and the obtained values are highly reproducible from experimental data. Although the signs of the atomic coordinates remain undetermined, they can typically be deduced easily from computational calculations.

The resulting parameters from the Kraitchman equations are compared with the equilibrium structure obtained with B3LYP-D3BJ/def2-TZVP in Table 3.

Rotational spectra have permitted the derivability of other empirical structures such as effective structure. However, their precision can be limited, especially when dealing with large amplitude motions. A comparison of the effective structure obtained using the spectroscopic parameters of all isotopologues is reported in the supplementary material.

To our knowledge, the structure of this molecule in condensed phases has been solely determined by X-ray diffraction analysis. Initially, in a room temperature experiment [32], the precise position of the hydrogen atom in the hydroxyl group was not determined. Subsequently, an experiment conducted at 110 K [33] estimated the dihedral angle between C6-C1-O-H to be −0.4(14)°. This flatness measurement aligns with theoretical calculations and the crystal structures of other phenols with different substitutions. Consequently, disregarding the hydrogen atom, the molecule exhibits approximate C_{2v} symmetry.

In accordance with the structure reported in the referenced article, Fig. 3 demonstrates a good agreement when superimposing the X-ray structure by the structure obtained through rotational spectroscopy. Thus, it can be confidently stated that the molecular conformation in the gas phase coincides with the crystal structure, with the positions of the carbon atoms in the tert-butyl groups accurately determined. Additionally, it is noteworthy that the X-ray diffraction data does not exhibit crystal packing effects, probably due to the fact that the bulky *tert*-butyl group prevents close contacts between vicinal hydroxyl groups, shielding the polar group and hindering long intermolecular interactions.

3.3. Intramolecular dynamics

The rotational spectrum of the parent species is predominantly affected by a tunnelling motion between the equivalent positions of the hydrogen atom of the hydroxyl group, causing a spectral splitting of approximately 190 MHz. This tunnelling phenomenon shares similarities with the splitting observed in phenol, albeit at a different separation of around 60 MHz. Several models have been proposed to explain the phenomenon in phenol, including motion of the hydroxyl group above and below the ring plane. Currently, our understanding aligns with a motion attributed to the two equivalent positions of the hydroxyl group within the ring plane. In this approximation, the experimental data are well reproduced by considering a double minimum potential function with a barrier of $V_2 = 1200\ cm^{-1}$ [14].

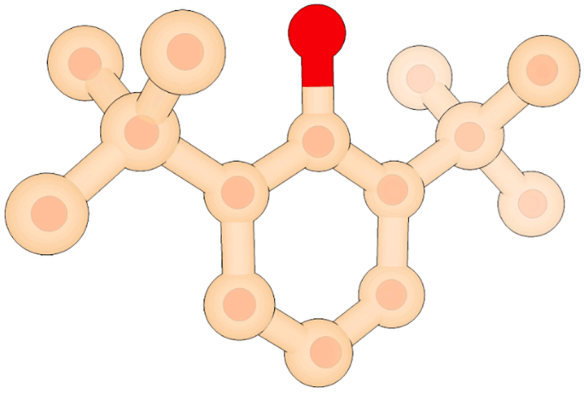

Fig. 3. The experimental X-ray structure of the 26BP superimposed with the determined r_s positions of the carbon atoms (red spheres).

It is interesting to note that also the spectrum of the most stable conformer of propofol (2,6-diisopropylphenol), whose two isopropyl groups have a plane-symmetric *gauche* orientation (Gg), is characterized by tunnelling splitting associated with the internal rotation of the hydroxyl group of about 104 MHz. The hindering barriers, for OH faced to the H atoms or *tert*-butyl groups are calculated to be 995 and 1035 cm^{-1}, respectively, at the MP2/6–311++*G*(d,p) level of theory or 905 and 940 cm^{-1}, respectively, if estimated with a relaxed flexible model [18].

Regarding 26BP, the observation of interstate transitions in the μ_a component and exclusively intrastate transitions in the μ_b component supports the notion that the motion stems from the internal rotation of the hydroxyl group. The potential function describing this motion can be modelled as a function with two equivalent symmetric minima, where the hydroxyl hydrogen is coplanar with the benzene ring. This motion is also corroborated by the number of observed ^{13}C isotopologues (12 out of 14 possible), their relative intensities varying with position (C8&C10 carbons being equivalent, as well as C12&C14, with their intensities doubled compared to the other isotopologues), and the maintenance of splitting for positions that do not alter the molecular symmetry relative to the parent species (C1 and C4).

In order to quantify this internal motion and reproduce the experimental data, it was decided to model the OH internal rotation potential function with the monodimensional flexible model of Meyer [34]. In short, the model considers that molecules exhibiting a large-amplitude motion can be described with a monodimensional potential function that controls this intramolecular dynamics. The rotational motion of the hydroxyl group can be described by using a two-fold potential function:

$$V(\tau) = 1/2V_2 \cdot [1 - \cos(2 \cdot \tau)] \quad (3)$$

where τ is the torsional coordinate (C2-C1-O-H) and V_2 is the barrier between the equivalent minima. As regards the other structural parameters, they were fixed to the theoretical predictions (B3LYP-D3BJ/def2-TZVP), imposing a C_{2v} arrangement to all the atoms except the hydroxyl hydrogen atom. This model reproduces the splitting (189.72 cm^{-1}) when the barrier is 890 cm^{-1}. Moreover, if we consider the mass increase obtained by deuterating the hydroxyl group, the model foresees a reduction of the splitting to 50 MHz. This model can be directly compared with the one developed to deal with the motion of the hydroxyl group of phenol.

Inspection of the theoretical double-minimum torsional potential function obtained both at the B3LYP-D3BJ/def2-TZVP and MP2/6–311++*G*(d,p) levels of theory with a scan of the dihedral angle τ steps of 10° (Fig. 4) shows that the minimum wells and barriers are slightly wider and narrower, respectively, than those depicted by the model function (Eq. (3)). This effect can be taken into account adding a negative V_4 term, as follows:

$$V(\tau) = 1/2V_2 \cdot [1 - \cos(2 \cdot \tau)] + 1/2V_4 \cdot [1 - cos(4 \cdot \tau)] \quad (4)$$

Actually, a good agreement can be found using V_2= 979 cm^{-1} and V_4= −104 cm^{-1} for DFT data and V_2= 807 cm^{-1} and V_4= −183 cm^{-1} for the ab initio ones.

However, given one experimental energy splitting it is not possible to fit both the parameters independently, but we can find a series of pairs that reproduce the splitting. The corresponding curves in Fig. 4 show that as V_4 becomes more negative, the barrier height increases to keep the splitting constant. Therefore, the value obtained with the simplest model (black curve, Eq. (3)) represents the lower limit for the hydroxyl internal rotation barrier (V_2·= 890 cm^{-1}), whose value can be estimated as 1000(100) cm^{-1}. It is worth noting that the introduction of structural relaxation in the model could change this estimation.

The calculated barrier for 26BP turns out to be slightly lower than for phenol itself. This could indicate that there is a high steric repulsion the hydroxyl group and the methyl of the tert-butyl groups. The same instability is associated with the known fact that the strength of the O—H bond is weaker if bulky substituents like tert-butyl groups are introduced in ortho positions of the benzenic ring [35]. In fact, the radical formed from the cleavage of this bond is more stabilised than other phenols, providing the antioxidant properties described in the introduction.

Although the main splitting has been understood, the phenomenon of splitting each individual interstate transition into three components, spaced a few kHz apart, remains unexplained. As depicted in Fig. 3, this splitting of transitions appears regular throughout the measurement range, with lower intensity transitions at the extremes and higher intensity transitions in the central positions of each triplet. The relative intensity ratio across all transitions remains approximately 0.7:1:0.2 on average. Various attempts have been made to explain this phenomenon, including modelling the potential rotation of tert-butyl groups [36,37]. However, this phenomenon remains presently elusive. The current motion exhibited by 26BTP alone, with its unique characteristics, appears to be beyond the scope of conventional Hamiltonians. Consequently, a comprehensive investigation and advanced implementation of the permutation-inversion group theory will be necessary to interpret and model the potential large-amplitude motion associated with the hydroxyl group's tunnelling [38].

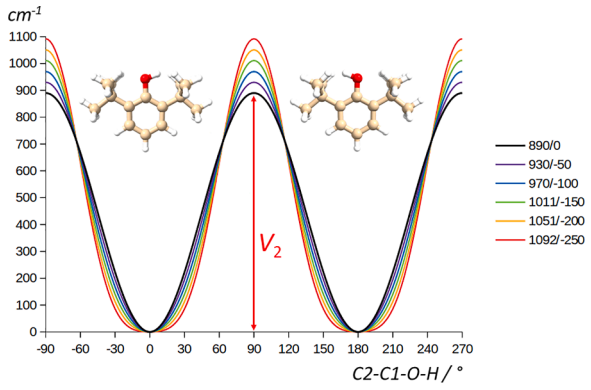

Fig. 4. Schematic diagram of the double-minimum torsional potential function of 26BP and possible flexible model potential energy functions that reproduce the observed splitting (the corresponding V_2 and V_4 values are given in the legend). The two conformations of 26BP correspond to two equivalent potential minima.

4. Conclusions

Our analysis of the rotational spectrum of 26BP has revealed multiple tunnelling effects, primarily due to the torsional motion associated with the hydroxyl group. Each transition is further split into three components, effectively interpreted as pairs of torsional states. The fitting of transitions was accomplished using a semirigid-rotor Hamiltonian and a two-state torsion-rotation coupled Hamiltonian, providing specific torsional energy differences and Coriolis coupling terms.

Regarding the molecular structure, rotational spectroscopy enabled the observation of isotopologues and their respective spectroscopic parameters. Replacement of specific carbons resulted in distinct spectra for each isotopologue, highlighting the symmetry group of the molecule. Comparisons with Kraitchman equations and X-ray analysis confirmed the accurate determination of the carbon skeleton.

The intramolecular dynamics of 26BP involved the tunnelling motion between the equivalent positions of the hydroxyl group. The potential function modelling internal rotation described the experimental data satisfactorily, with a double minimum potential function and a barrier between equivalent minima of ~1000(100) cm^{-1}. However, the splitting of each individual transition into three components remained unexplained, requiring further investigation using the permutation-inversion group theory to interpret the large-amplitude motions associated to both the hydroxyl and tertbutyl group tunnelling.

CRediT authorship contribution statement

Wenqin Li: Investigation, Writing – review & editing. **Assimo Maris:** Conceptualization, Methodology, Formal analysis, Writing – review & editing. **Sonia Melandri:** Methodology, Writing – review & editing. **Alberto Lesarri:** Methodology, Formal analysis, Resources, Writing – review & editing, Supervision, Funding acquisition. **Luca Evangelisti:** Conceptualization, Methodology, Formal analysis, Resources, Writing – original draft, Writing – review & editing, Funding acquisition.

Declaration of Competing Interest

The authors declare that they have no known competing financial interests or personal relationships that could have appeared to influence the work reported in this paper.

Data availability

Data are available in the Supplementary material.

Acknowledgements

W. L. thanks the China Scholarships Council (CSC) for a scholarship. We acknowledge the CINECA award under the ISCRA initiative, for the availability of high-performance computing resources and support. This work was supported by University of Bologna (RFO) and Fondazione Cassa di Risparmio di Bologna. W.L., and A.L. acknowledge funding from the Ministerio de Ciencia e Innovación and European Regional Development Fund (ERDF) through grant PID2021-125015NB-I00, and the Junta de Castilla y León - ERDF grants INFRARED IR2020-1-UVa02 and INFRARED IR2021-UVa13.

Supplementary materials

Supplementary material associated with this article can be found, in the online version, at doi:10.1016/j.molstruc.2023.136910.

References

[1] D. Calabria, M. Guardigli, P. Severi, I. Trozzi, A. Pace, S. Cinti, M. Zangheri, M. Mirasoli, A smartphone-based chemosensor to evaluate antioxidants in agri-food matrices by *in situ* AuNP formation, Sensors 21 (16) (2021) 5432.
[2] M. Parcheta, R. Świsłocka, S. Orzechowska, M. Akimowicz, R. Choińska, W. Lewandowski, Recent developments in effective antioxidants: the structure and antioxidant properties, Materials 14 (8) (2021) 1984.
[3] E.D.N.S. Abeyrathne, K. Nam, X. Huang, D.U. Ahn, Plant-and animal-based antioxidants' structure, efficacy, mechanisms, and applications: a review, Antioxidants 11 (5) (2022) 1025.
[4] J. Neill, L. Evangelisti, B.H. Pate, Analysis of isomeric mixtures by molecular rotational resonance spectroscopy, Anal. Sci. Adv. 4 (2023) 204–219.
[5] I. Pena, A.M. Daly, C. Cabezas, S. Mata, C. Bermudez, A. Nino, J.C. Lopez, J. U. Grabow, J.L. Alonso, Disentangling the puzzle of hydrogen bonding in vitamin C, J. Phys. Chem. Lett. 4 (1) (2013) 65–69.
[6] A. Vigorito, C. Calabrese, E. Paltanin, S. Melandri, A. Maris, Regarding the torsional flexibility of the dihydrolipoic acid's pharmacophore: 1, 3-propanedithiol, Phys. Chem. Chem. Phys. 19 (1) (2017) 496–502.
[7] G. Salvitti, E. Pizzano, F. Baroncelli, S. Melandri, L. Evangelisti, F. Negri, M. Coreno, K.C. Prince, A. Ciavardini, H. Sa'adeh, M. Pori, Spectroscopic and quantum mechanical study of a scavenger molecule: N, N-diethylhydroxylamine, Spectrochim. Acta Part A 281 (2022), 121555.
[8] F. Baroncelli, G. Panizzi, L. Evangelisti, S. Melandri, A. Maris, Structure and nuclear quadrupole coupling interaction in hydroxylamines: the rotational spectrum of N, N-diethyl (2H) hydroxylamine, J. Mol. Spectrosc. 392 (2023), 111759.
[9] G. Salvitti, F. Baroncelli, C. Nicotri, L. Evangelisti, S. Melandri, A. Maris, How water interacts with the NOH Group: the rotational spectrum of the 1: 1 N, N-diethylhydroxylamine·Water Complex, Molecules 27 (23) (2022) 8190.
[10] J.M. Lü, P.H. Lin, Q. Yao, C. Chen, Chemical and molecular mechanisms of antioxidants: experimental approaches and model systems, J. Cell. Mol. Med. 14 (4) (2010) 840–860.
[11] N.W. Larsen, E. Mathier, A. Bauder, H.H. Günthard, Analysis of microwave and infrared transitions of phenol by rotation-internal rotation theory. Phenol-OD, J. Mol. Spectrosc. 47 (2) (1973) 183–188.
[12] C. Tanjaroon, S.G. Kukolich, Measurements of the rotational spectra of phenol and 2-pyrone and computational studies of the H-bonded phenol− pyrone dimer, J. Phys. Chem. A 113 (32) (2009) 9185–9192.
[13] L. Kolesniková, A.M. Daly, J.L. Alonso, B. Tercero, J. Cernicharo, The millimeter wave tunneling–rotational spectrum of phenol, J. Mol. Spectrosc. 289 (2013) 13–20.
[14] Z. Kisiel, Further rotational spectroscopy of phenol: sextic centrifugal distortion and vibrational satellites, J. Mol. Spectrosc. 386 (2022), 111630.
[15] N.W. Larsen, Microwave spectra and internal rotation of 4-fluorophenol, 4-chlorophenol and 4-bromophenol, J. Mol. Struct. 144 (1–2) (1986) 83–99.
[16] N.W. Larsen, L. Schulz, Internal rotation and structure of thiophenol and 4-fluorothiophenol studied by microwave spectroscopy and quantum chemistry, J. Mol. Struct. 920 (1–3) (2009) 30–39.
[17] W. Li, R.T. Saragi, M. Juanes, J. Demaison, N. Vogt, A. Fernández-Ramos, A. Lesarri, Equilibrium structures of selenium compounds: the torsionally flexible molecule of selenophenol, J. Chem. Phys. 159 (2) (2023), 024303.
[18] A. Lesarri, S.T. Shipman, J.L. Neill, G.G. Brown, R.D. Suenram, L. Kang, W. Caminati, B.H. Pate, Interplay of phenol and isopropyl isomerism in propofol from broadband chirped-pulse microwave spectroscopy, J. Am. Chem. Soc. 132 (38) (2010) 13417–13424.
[19] G.G. Brown, B.C. Dian, K.O. Douglass, S.M. Geyer, S.T. Shipman, B.H. Pate, A broadband Fourier transform microwave spectrometer based on chirped pulse excitation, Rev. Sci. Instrum. 79 (5) (2008), 053103.
[20] A.D. Becke, Density-functional thermochemistry. III. The role of exact exchange, J. Chem. Phys. 98 (7) (1993) 5648. -6.
[21] M.J. Frisch, G.W. Trucks, H.B. Schlegel, G.E. Scuseria, M.A. Robb, J.R. Cheeseman, G. Scalmani, V. Barone, G.A. Petersson, H. Nakatsuji, X. Li, Gaussian 16 Revision C. 01, 2016, Gaussian Inc, Wallingford CT, 2016, p. 421.
[22] S. Grimme, S. Ehrlich, L. Goerigk, Effect of the damping function in dispersion corrected density functional theory, J. Comput. Chem. 32 (7) (2011) 1456–1465.
[23] E.R. Johnson, A.D. Becke, A post-Hartree-Fock model of intermolecular interactions: inclusion of higher-order corrections, J. Chem. Phys. 124 (17) (2006), 174104.
[24] F. Weigend, R. Ahlrichs, Balanced basis sets of split valence, triple zeta valence and quadruple zeta valence quality for H to Rn: design and assessment of accuracy, Phys. Chem. Chem. Phys. 7 (18) (2005) 3297–3305.
[25] M. Juanes, I. Usabiaga, I. León, L. Evangelisti, J.A. Fernández, A. Lesarri, The six isomers of the cyclohexanol dimer: a delicate test for dispersion models, Angew. Chem. Int. Ed. 59 (33) (2020) 14081–14085.
[26] K. Mayer, C. West, F.E. Marshall, G. Sedo, G.S. Grubbs, L. Evangelisti, B.H. Pate, Accuracy of quantum chemistry structures of chiral tag complexes and the assignment of absolute configuration, Phys. Chem. Chem. Phys. 24 (45) (2022) 27705–27721.
[27] C. Møller, M.S. Plesset, Note on an approximation treatment for many-electron systems, Phys. Rev. 46 (7) (1934) 618.
[28] J.K. Watson, J.R. Durig (Ed.), In, Vibrational Spectra and Structure, 6, Elsevier, Amsterdam, 1977, pp. 1–89. Vol..
[29] H.M. Pickett, The fitting and prediction of vibration-rotation spectra with spin interactions, J. Mol. Spectrosc. 148 (2) (1991) 371–377.
[30] J. Kraitchman, Determination of molecular structure from microwave spectroscopic data, Am. J. Phys. 21 (1) (1953) 17–24.
[31] L. Evangelisti, C. Perez, N.A. Seifert, B.H. Pate, M. Dehghany, N. Moazzen-Ahmadi, A.R.W. McKellar, Theory vs. experiment for molecular clusters: spectra of OCS trimers and tetramers, J. Chem. Phys. 142 (10) (2015), 104309.
[32] M. Lutz, A.L. Spek, 2, 6-Di-tert-butylphenol revisited at 110 K, Acta Crystallogr. Sect. C Cryst. Struct. Commun. 61 (11) (2005) o639–o641.
[33] G.G. Lazarev, V.L. Kuskov, Y.S. Lebedev, W. Hiller, M. Kretschmar, A. Rieker, Mechanism of radical pair formation during the photolysis of 2, 6-di-tert-butyl-quinonediazide in single crystals of 2, 6-di-tert-butylphenol, Z. Phys. Chem. 176 (1) (1992) 41–46.
[34] R. Meyer, Flexible models for intramolecular motion, a versatile treatment and its application to glyoxal, J. Mol. Spectrosc. 76 (1–3) (1979) 266–300.
[35] M. Lucarini, P. Pedrielli, G.F. Pedulli, S. Cabiddu, C. Fattuoni, Bond dissociation energies of O− H bonds in substituted phenols from equilibration studies, J. Org. Chem. 61 (26) (1996) 9259–9263.
[36] H. Hartwig, H. Dreizler, The microwave spectrum of trans-2, 3-dimethyloxirane in torsional excited states, Z. Naturforsch. A 51 (8) (1996) 923–932.
[37] V. Ilyushin, R. Rizzato, L. Evangelisti, G. Feng, A. Maris, S. Melandri, W. Caminati, Almost free methyl top internal rotation: rotational spectrum of 2-butynoic acid, J. Mol. Spectrosc. 267 (1–2) (2011) 186–190.
[38] J.T. Hougen, Strategies for advanced applications of permutation–inversion groups to the microwave spectra of molecules with large amplitude motions, J. Mol. Spectrosc. 256 (2) (2009) 170–185.